Permeability of Dawson–type polyoxometalates through vertically oriented nanoporous silica membranes on electrode: Effect of pore size and probe charge

Neus Vilà, Pedro de Oliveira, Alain Walcarius, Israël Mbomekallé

Permeability of Dawson–type polyoxometalates through vertically oriented nanoporous silica membranes on electrode: Effect of pore size and probe charge

Neus Vilà,*[a] Pedro de Oliveira,[b] Alain Walcarius[a] and Israël M. Mbomekallé*[b]

[a] *Université de Lorraine, CNRS, LCPME, F-54000 Nancy, France*[§]

[b] *Equipe d'Electrochimie et Photo-électrochimie, Institut de Chimie Physique, UMR 8000 CNRS, Université Paris Saclay, Orsay F-91405, France*

* E-mail : neus.vila@univ-lorraine.fr, israel.mbomekalle@universite-paris-saclay.fr

[§] *Postal address: Laboratoire de Chimie Physique et Microbiologie pour les Matériaux et l'Environnement, 405 rue de Vandoeuvre, 54600 Villers-lès-Nancy, France*

Abstract

The voltammetric behavior of bulky heteropolyanions belonging to the Dawson family of polyoxometalates, $[P_2V_mW_{18-m}O_{62}]^{n-}$ (m = 0, 3, 6), has been investigated at electrodes coated with vertically-aligned mesoporous silica thin films with pore openings in the 2-3 nm range. The experiments have been carried out in acidic medium (pH 0.3-1), where the silica surface is positively charged and thus likely to interact with the negatively charged redox probes, and at various ionic strengths of the medium. Better permeability of the films was clearly observed at lower pH values, corresponding to higher densities of positive charges onto the silica walls, and of films with a larger mesopore size, favoring the mass transport rates through the nanoporous membrane. Diffusion of such bulky anionic redox probes was dramatically influenced by the ionic strength of the medium, being especially restricted at low electrolyte concentrations where the thickness of the electrical double layer became of the same order of magnitude or larger than the mesopore radius, giving rise to very low voltammetric signals. The overall negative charge on POMs had few effects on their mass transport through the film, except at low ionic strength where the most highly charged redox probes gave rise to the lowest current responses.

Keywords: Mesoporous silica film electrode, polyoxometalates, permeability, mass transport, cyclic voltammetry at membrane electrodes

1. Introduction

Polyoxometalates (POMs) are molecular oxides made of transition metals at high oxidation state and oxygen, often containing heteroatoms, existing mainly in the form of bulky heteropolyanions with nanosized geometry and exhibiting multi-electron transfer properties without structure variation [1-3]. Thanks to their very rich electrochemistry [2, 4], these heteropolyanions of general formula $[X_xM_mO_y]^{n-}$ (with X the heteroatom and M the metal atom) have found many applications as electrocatalysts, notably for electrochemical sensing and energy storage and conversion applications [4-7]. For practical uses, POMs often need to be confined onto electrode surfaces, which can be notably achieved via chemisorption, electrodeposition, encapsulation in polymers or inorganic matrices, and deposition as monolayers (Langmuir-Blodgett process) or multilayers (layer-by-layer assembly) [6, 8-12]. A controlled spatial arrangement (i.e., regular distribution at the nanoscale) might be also of interest to promote efficient charge transfer processes [13].

From that point of view, the ordered mesoporous silicate-based materials (i.e., as prepared using supramolecular assemblies as template [14]) appear to be suitable hosts for POM confinement, as exemplified by the elaboration of heterogeneous POM-containing mesoporous catalysts [15-18], with immobilization strategies involving either electrostatic interactions [16] or covalent bonding [17]. Mesoporous materials can be manufactured in the form of thin films on solid supports [19] and such configuration has been largely exploited in electrochemistry [20]. POMs have been previously accommodated to such mesoporous films on electrode and subsequently used for electrochemical applications [21-23]. One key parameter affecting the electrochemical response of mesoporous silica modified electrodes is the accessibility to the electrode surface and thus the mass transport through the nanoporous film [24]. This can be significantly influenced by the film characteristics (such as structure, pore size, hydrophobic/hydrophilic balance, or thickness [25-29]) or by solution parameters (such as pH and ionic strength or probe charge and size [25, 29-34]). An attractive mesostructure geometry is achieved in mesoporous silica films made of a dense hexagonal packing of mesopore channels all oriented vertically with respect to the underlying electrode surface, which can be easily generated by electro-assisted self-assembly [35, 36], because it offers the most direct access to solution-phase species. Indeed, well-ordered one-dimensional (1D) mesopores that guide and confine the motions of reagents or analytes is often required to achieve optimal material performance in many applications. If the structure and orientation of such aligned nanoporous silica membranes can be easily characterized by grazing-incidence small-angle scattering and transmission

electron microscopy [37-39], accurate information on their permeation to external reagents or analytes is also necessary. Besides geometric considerations, the film permeability in solution-phase applications depends upon the distribution of the analytes to regions nearest the pore walls [33, 34]. The relative polarities of the solute molecules, silica pore walls, and pore-filling medium are all key factors expected to govern the partitioning processes. The charge carried by the molecules and the pore surface and the thickness of the diffuse electrical double layer within the pore are also important [31-34]. To date, most investigations have been performed on the basis of small redox probes and we would like to extend it to bulkier ionic species.

In a previous paper [40], we started studying the voltammetric response of a bulky polyanion (a Keggin-type POM, $[SiW_{12}O_{40}]^{4-}$) at an electrode modified with a vertically-aligned mesoporous silica thin film. It came out that pH values below the point of zero charge of the silica (i.e., < 2-3, corresponding to positively-charged silica walls) were necessary to get significant current responses due to favourable electrostatic interactions and that the ionic strength of the medium played an important role in modulating the thickness of the electrical double layer in the mesopore channels. On the basis of these preliminary observations, we would like to go one step further by considering the effect of the mesopore size and the probe charge. POMs are nanometric anions with many delocalized charges, but their overall charge densities are low and their polarizabilities are expected to be high. Here, we have thus evaluated a series of Dawson-type POMs ($[P_2W_{18}O_{62}]^{6-}$, $[P_2V_3W_{15}O_{62}]^{9-}$ and $[P_2V_6W_{12}O_{62}]^{12-}$), i.e., a bit larger than the Keggin one and bearing distinct charge densities, at electrodes coated with vertically oriented mesoporous silica films exhibiting two different pore diameters (2-3 nm range). Using cyclic voltammetry, the goal is to show how the mass transport of such bulky redox heteropolyanions through the mesoporous film is affected by these parameters (pore size and POM charge) as a function of the pH and the ionic strength of the medium.

2. Experimental section

2.1. Chemicals and reagents

Tetraethoxysilane (TEOS, 98%, Alfa Aesar), ethanol (95-96%, Merck), $NaNO_3$ (98%, Prolabo), HCl (37% Riedel de Haen), cetyltrimethylammonium bromide (CTAB, 99%, Acros) and octadecyltrimethylammonium bromide (ODAB) have been used as received. Pure samples of $K_6[P_2W_{18}O_{62}].20H_2O$, $K_9[P_2V_3W_{15}O_{62}].20H_2O$ and $K_9[P_2V_6W_{12}O_{62}].20H_2O$ (see their structures in part A of Figure 1) were prepared by following a synthetic procedure previously

reported for octadecatungstodiphosphates and related lacunary compounds [41-43]. They were dissolved at the desired concentration in aqueous solutions containing H_2SO_4 and variable amounts of Na_2SO_4 as supporting electrolyte.

2.2. Preparation of vertically-aligned mesoporous silica thin films

The vertically-oriented silica thin films have been electrochemically generated on indium-tin oxide (ITO) electrodes according to the previously reported EASA procedure [36]. A hydroalcoholic solution (10 mL H_2O + 10 mL EtOH) containing 100 mM of the silica precursor (TEOS), 32 mM of surfactant template (CTAB or ODAB) and 0.1 M of electrolyte ($NaNO_3$), was prepared and its pH was adjusted to 3 by adding 0.1 M HCl. After a first step of hydrolysis for 2.5 h, a cathodic potential of -1.3 V was applied for 20 s to the ITO working electrode to initiate the oriented growth of the mesoporous silica layer. The film electrode was thoroughly rinsed with water and aged overnight at 130°C. The extraction of the surfactant template was achieved by immersing the film electrode in an ethanol solution containing 0.1 M HCl for 15 min. Their hexagonal mesostructure and vertical pore orientation were confirmed by Transmission Electron Microscopy (see illustrations in part B of Figure 1). They were characterized by a thickness of 95 nm and mesopore sizes of 2.1 and 2.9 nm (respectively for films prepared from CTAB and ODAB surfactants), in agreement with previous observations made for similar nanoporous silica membranes [29].

2.3. Apparatus

Both film syntheses and electrochemical characterizations were performed using an EG & G 273 A potentiostat/galvanostat driven by a PC with the M270 software (Princeton Applied Research, Ametek, France). A home-made electrochemical cell was used for film synthesis [44]. A one-compartment cell with a standard three-electrode configuration was used for cyclic voltammetry experiments. The reference electrode was a saturated calomel electrode (SCE) separated from the bulk electrolyte solution via fritted compartments filled with the same electrolyte. The counter electrode was a platinum gauze of large surface area. The working electrode was an indium-tin oxide plate coated, or not, with a mesoporous silica film. Cyclic voltammograms have been recorded at 20 mV s^{-1} (unless specified otherwise) from aqueous solutions of the POM at selected pH values and ionic strengths adjusted using H_2SO_4 and/or Na_2SO_4.

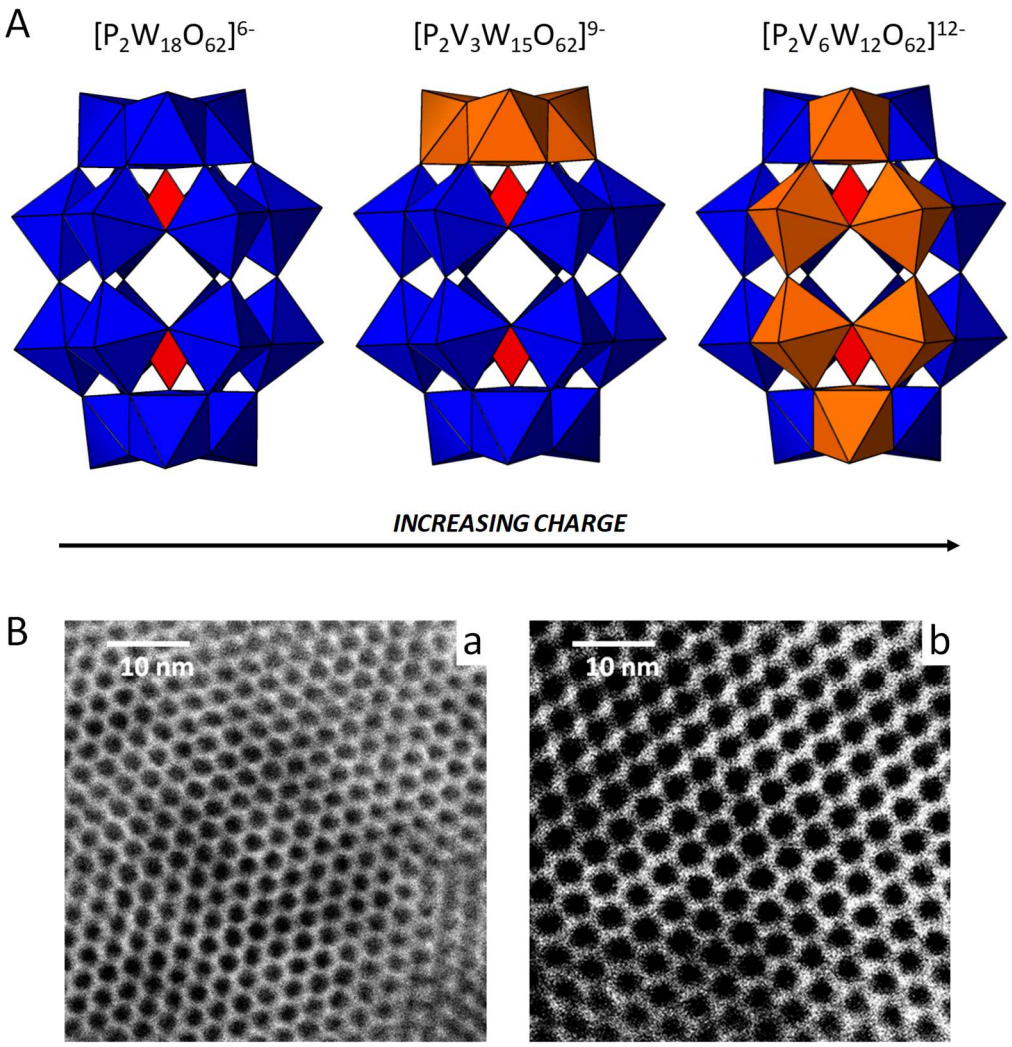

Figure 1. (A) Representative structure of the heteropolyanions studied: $[P_2W_{18}O_{62}]^{6-}$, $[P_2V_3W_{15}O_{62}]^{9-}$ and $[P_2V_6W_{12}O_{62}]^{12-}$. (B) TEM micrographs obtained for mesoporous silica films prepared from (a) CTAB and (b) ODAB surfactant templates.

3. Results and Discussion

Taking into account the amphoteric character of silica, the surface of mesopore walls can be either positive (due to the presence of $\equiv SiOH_2^+$ functions) at pH < 2, neutral (mainly $\equiv SiOH$ groups) at pH 2-3 or negative (due to $\equiv SiO^-$ moieties) at pH > 3 [45]. As a consequence, redox-active anions are likely to accommodate the film to reach the ITO surface primarily in acidic media, while being charge-excluded when the silica walls become negative due to electrostatic repulsions [32, 40]. The films permeability properties with respect to $[P_2V_mW_{18-m}O_{62}]^{n-}$ (m = 0, 3, 6) derivatives have been investigated here at pH 0.3 and 1.0 using cyclic voltammetry (CV).

3.1. Electrochemical behavior of Dawson-type POMs on bare ITO

Figure 2 shows typical CV curves recorded at a bare ITO electrode for the three POMs at the two pH values (0.3 and 1.0). The electrochemical behavior of $[P_2W_{18}O_{62}]^{6-}$ is well-established, yet at carbon electrodes [2, 46, 47], and its behavior was the same on ITO (Fig. 2A). It involves four reversible redox processes associated with the reduction of the tungsten-oxo framework: two initial reversible single-electron processes (I and II) followed by two bi-electronic steps (III and IV). The peak potentials for I and II are essentially independent of pH; by contrast, those for the third and fourth processes shifted to more negative values with increasing pH, in agreement with the following equations:

$[P_2W_{18}O_{62}]^{6-} + 1e^- \rightarrow [P_2W_{18}O_{62}]^{7-}$ Process I

$[P_2W_{18}O_{62}]^{7-} + 1e^- \rightarrow [P_2W_{18}O_{62}]^{8-}$ Process II

$[P_2W_{18}O_{62}]^{8-} + 2e^- + 2H^+ \rightarrow [H_2P_2W_{18}O_{62}]^{8-}$ Process III

$[H_2P_2W_{18}O_{62}]^{8-} + 2e^- + 2H^+ \rightarrow [H_4P_2W_{18}O_{62}]^{8-}$ Process IV

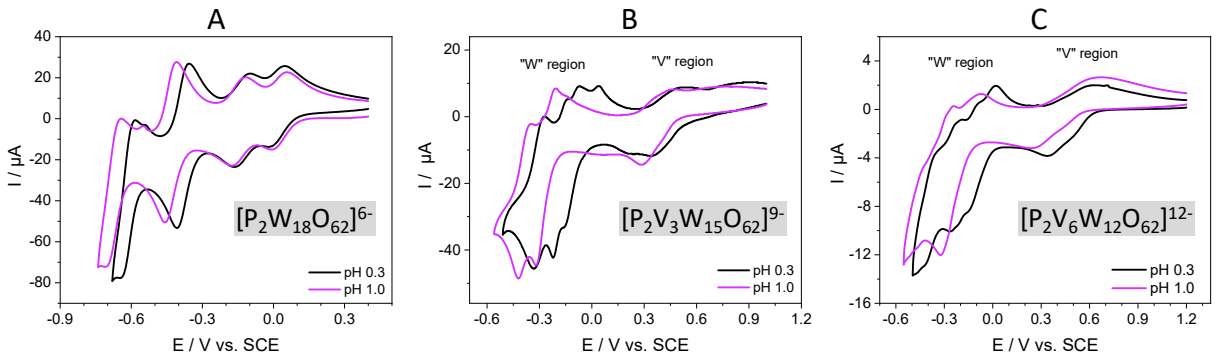

Figure 2. Voltammograms recorded in 0.5 mM $[P_2W_{18}O_{62}]^{6-}$ (A), $[P_2V_3W_{15}O_{62}]^{9-}$ (B) or $[P_2V_6W_{12}O_{62}]^{12-}$ (C) at a bare ITO electrode, in H_2SO_4 solutions at pH 0.3 (black curves) and 1.0 (violet curves), at 20 mV s^{-1}. Working electrode area: 0.125 cm^2

The electrochemical behavior of the $[P_2V_3W_{15}O_{62}]^{9-}$ and $[P_2V_6W_{12}O_{62}]^{12-}$ species was much less investigated [48], but one can see from their CV curves (respectively parts B&C in Fig. 2) that they are characterized by two regions corresponding to the reduction of vanadium centers (at ca. 0.5-0.3 V) followed by the reduction of tungsten centers at more cathodic positions (below 0 V) with potentials shifting to more negative values with increasing pH, suggesting again the involvement of protons in the reduction processes. The redox steps have been elucidated for the reduction of $[P_2V_3W_{15}O_{62}]^{9-}$, suggesting a very close sequence of two electron

transfer steps, one being two-electron and the other single-electron (corresponding to the reduction of the three V^{V} centers into V^{IV}), followed by two distinct four-electron and two-electron processes (corresponding to the reduction of the W centers), and $[P_2V_6W_{12}O_{62}]^{12-}$ seems to behave similarly [48]. The determination of the exact electron transfer mechanisms was beyond the scope of the present work, as we are primarily interested in comparing the relative intensities of CV current responses when passing from bare ITO to the mesoporous silica film modified electrodes.

3.2. Electrochemical behavior of Dawson-type POMs on a mesoporous silica film electrode

When using ITO electrodes coated with the large pore mesoporous silica film (2.9 nm in diameter) and operating at pH 0.3, a significant increase in the current responses was observed, as illustrated in Figure 3. These curves were obtained after template removal, as no electrochemical signal can be observed prior to ODAB surfactant extraction (data not shown, but totally in agreement with previous works reporting electrochemical studies of ionic redox probes at such mesoporous silica film electrodes [32, 49]). The almost two-fold current increase (I_{film}/I_{bare} ~ 1.8-2.0) in the presence of the film indicates the accumulation of the negatively-charged POMs via favorable electrostatic interactions with the positively-charged silica surface of the mesochannels, with approximately the same efficiency independently on the nature of the heteropolyanion, yet perhaps with a slightly better effectiveness of the process for more charged POMs, but the variation is of the magnitude of the measurement error (I_{film}/I_{bare} = 1.8±0.1 for $[P_2W_{18}O_{62}]^{6-}$, 2.0±0.1 for $[P_2V_3W_{15}O_{62}]^{9-}$ and 1.9±0.1 for $[P_2V_6W_{12}O_{62}]^{12-}$). Current enhancement was observed for all redox processes of the various probes. As I_{film} is proportional to $D_{film}^{1/2}\times C_{film}$ (and I_{bare} to $D_{sol}^{1/2}\times C_{sol,}$ with sol = solution) according to the Randles-Sevcik equation [50], and assuming $D_{film} < D_{sol}$ (because of expected resistance to mass transport in such small nanochannels, in agreement with slower diffusion of electroactive species through other types of membranes such as poly(vinylferrocene) films [51, 52]), the results of Figure 3 indicate a quite high accumulation effectiveness ($C_{film} >> C_{sol}$). Nevertheless, no noticeable shift in the characteristic peak potentials can be seen, indicating rather weak interactions between POMs and the mesoporous silica matrix, in agreement with previous observations for $[P_2W_{18}O_{62}]^{6-}$ encapsulated in sol-gel films [10]. Stronger interactions would have resulted in potential shifts due to changes in the rate of electron transfer processes [53]. Also note that POM transport into the mesoporous films has not to be considered as pure physical diffusion and that diffusion coefficients (D_{film}) are actually “apparent diffusion coefficients” because of

these POM interactions with the silica walls. At the present stage of the investigation, this behavior is very similar as that previously observed for the Keggin-type POM probe, $[SiW_{12}O_{40}]^{4-}$ [40], which exhibited similar current enhancements (I_{film}/I_{bare} ~ 2) although its negative charge was lower and its size slightly smaller, but size effects will be further discussed in the following.

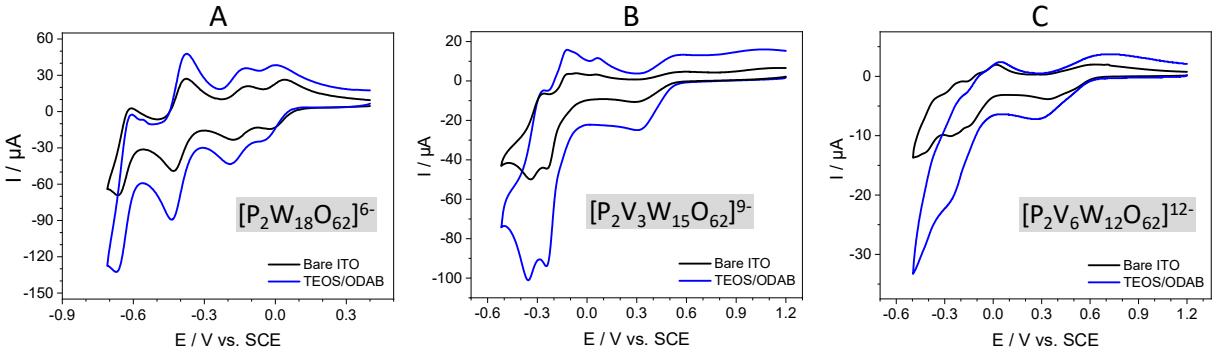

Figure 3. Voltammograms recorded in 0.5 mM $[P_2W_{18}O_{62}]^{6-}$ (A), $[P_2V_3W_{15}O_{62}]^{9-}$ (B) or $[P_2V_6W_{12}O_{62}]^{12-}$ (C) at an ITO electrode covered by an ODAB-based mesoporous silica film (blue curves), as obtained in 0.5 M H_2SO_4 (pH 0.3) at 20 mV s^{-1}. The voltammetric curves recorded on bare ITO are superimposed for comparison purpose (black curves). Working electrode area: 0.125 cm^2

3.3. Effect of the mesopore diameter and the probe size

Figure 4 (parts A&B) compares the voltammetric responses obtained for $[P_2W_{18}O_{62}]^{6-}$ using two film electrodes characterized by mesopore diameters of 2.1 nm (TEOS/CTAB film) and 2.9 nm (TEOS/ODAB film), respectively, at two pH values (0.3 and 1.0). As shown, for pH 0.3 (Fig. 4A), if the $[P_2W_{18}O_{62}]^{6-}$ species are likely to cross easily the ODAB-based film and even to be accumulated inside (I_{film}/I_{bare} = 1.8), their response at the CTAB-based film electrode was much less intense and even lower than at bare ITO (I_{film}/I_{bare} = 0.55). This can be explained by the smaller pore diameter of the CTAB-based film, inducing more resistance to mass transport through the silica nanochannels. This effect was even more noticeable and restrictive at pH 1.0 (Fig. 4B) for which the I_{film}/I_{bare} values are of ca. 0.6 and 0.2 (respectively for ODAB- and CTAB-based films). This clearly indicates a pH-influenced size selectivity of the mesoporous films.

For comparison purposes, the results obtained for the Keggin-type POM $[SiW_{12}O_{40}]^{4-}$ are also shown (Fig. 4C&D). They demonstrate the dramatic influence of the balance between mesopore

diameter and probe size on the voltammetric response of POMs at mesoporous silica film electrodes. Whereas a significant current enhancement can be observed at pH 0.3 for the smaller probe ($[SiW_{12}O_{40}]^{4-}$) at both films exhibiting pore entrances of 2.1 and 2.9 nm, only the larger nanochannels were likely to enable significant ingress of the slightly larger $[P_2W_{18}O_{62}]^{6-}$ probe (see blue curves in Fig. 4A&C for instance), while smaller nanochannels led to much more resistance to mass transport of $[P_2W_{18}O_{62}]^{6-}$ relative to $[SiW_{12}O_{40}]^{4-}$ (compare red curves in Fig. 4A&C). These features were observed for the two pH values investigated here (yet with less intense currents at pH 1.0, see explanation below): little effect of the mesopore diameter on the response of $[SiW_{12}O_{40}]^{4-}$ (Fig. 4C&D) as compared to the very different signals recorded for $[P_2W_{18}O_{62}]^{6-}$ at the two film electrodes, respectively prepared from CTAB or ODAB (Fig. 4A&B).

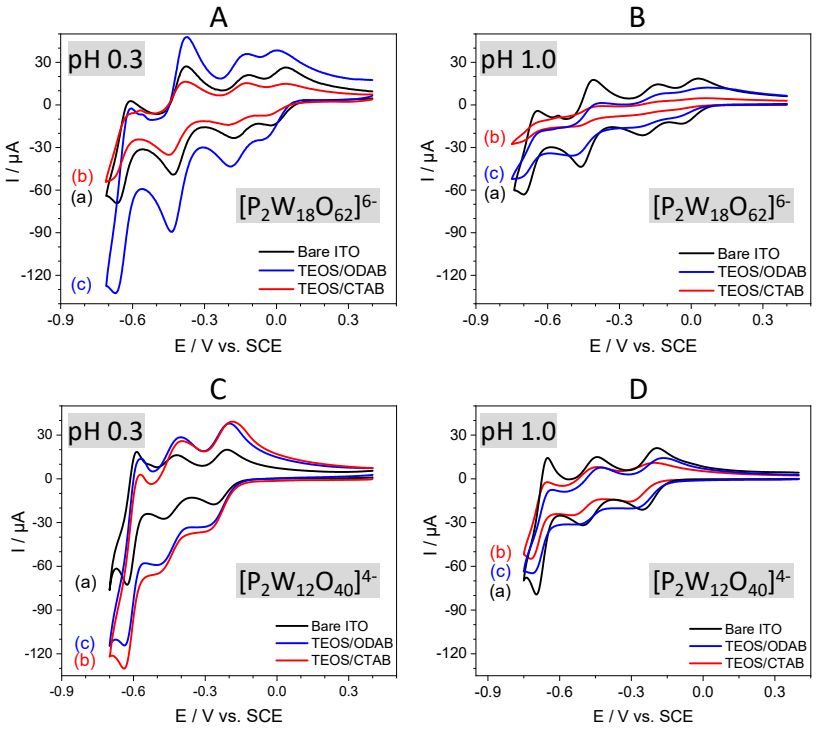

Figure 4. Voltammograms recorded in 0.5 mM $[P_2W_{18}O_{62}]^{6-}$ (A, B) or 0.5 mM $[SiW_{12}O_{40}]^{4-}$ (C, D) at bare ITO electrode (a) and ITO electrodes covered by CTAB-based (b) or ODAB-based (c) mesoporous silica films, respectively in H_2SO_4 solutions at pH 0.3 (A, C) and 1.0 (B, D), at 20 mV s^{-1}. Working electrode area: 0.125 cm^2

Differences observed between pH 0.3 and 1.0 can be explained by taking into account several parameters. At both pH values, the silica surface is positively charged [45] but the density of $\equiv SiOH_2^+$ groups onto the mesopore walls has been reported to be slightly higher at lower pH

[54], possibly contributing to the accumulation of more POM anions. However, this is certainly not the main reason leading to the big differences shown on Figure 4, as the silica surface state is expected to be mostly the same at a defined pH for both smaller and larger pore films. The mesopore diameter and probe size seem to play a major role. Actually, when adjusting the pH by tuning the concentration of a strong acid (H_2SO_4) as we did here, another parameter is evolving concomitantly, the ionic strength, thus affecting the electrical double layer (EDL) associated with the charged surface. The thickness of the electrical double layer can be estimated from the Debye length (λ_D), which can be calculated from equation 1:

$$\lambda_D = \sqrt{\frac{\varepsilon_0 \varepsilon_r K_B T}{2 N_A q^2 I}} \qquad (1)$$

where ε_0 is the vacuum permittivity (8.85×10^{-12} m^{-1}), ε_r is the relative permittivity of water (7.84×10^{-10} F m^{-1} at 25°C) also called dielectric constant, K_B is the Boltzmann constant (1.38×10^{-23} J K^{-1}), T is the temperature in K, q is the charge of an electron, I is the ionic strength and N_A is the Avogadro constant (6.02×10^{23} mol^{-1}).

According to equation 1, the Debye length is proportional to the reciprocal square root of the ionic strength. The larger the concentration of ions, the more they "shield" the charged surface and the thinner the Debye length is. This is illustrated in Figure 5 for the two media considered above (0.5 M H_2SO_4, pH 0.3, and 0.1 M H_2SO_4, pH 1.0) and the two film electrodes, respectively prepared from CTAB or ODAB (Fig. 5A). As shown, the same EDL thickness variation in smaller and larger mesopores does not have the same effect in terms of "effective pore diameter" (i.e., "pore size – 2λ" values) (Fig. 5B). This contributes to explain the big differences observed between the voltammetric responses of the Dawson $[P_2W_{18}O_{62}]^{6-}$ and Keggin $[SiW_{12}O_{40}]^{4-}$ POM probes at the two film electrodes and two pH values (Fig. 4). At pH 0.3 (Fig. 4A&C), both probes are likely to cross easily the large mesopore channels (as their "effective pore diameter" remain large, i.e. 2.0 nm, Fig. 5A) whereas noticeable restrictions appear for $[P_2W_{18}O_{62}]^{6-}$ at the smaller pore film ("effective pore diameter" of ca. 1.2 nm, Fig. 5A). This can be attributed to a slower mass transport of $[P_2W_{18}O_{62}]^{6-}$ through the nanochannels due to its obviously bigger size compared to $[SiW_{12}O_{40}]^{4-}$; for $[SiW_{12}O_{40}]^{4-}$ a hydrodynamic radius has been reported (R_H = 0.52 nm in H_2O + 250 mM NaCl [55]), corresponding to a sphere with diameter of 1.04 nm (consistent with its molecular size determined by X-ray crystallography [56-58]) and, even if no R_H data is available for $[P_2W_{18}O_{62}]^{6-}$, it should be significantly larger on the basis of crystallographic information (rugby ball-like shape with a

molecular size of ca. 1.1×1.45 nm for $[P_2W_{18}O_{62}]^{6-}$ [58-60]). At pH 1.0, mass transport processes were even more restrictive for both POMs, but much marked for the bigger heteropolyanion, especially for the smaller pore film (Fig. 4B&D). Interestingly, one can notice the very similar intensity of the voltammetric signals of $[P_2W_{18}O_{62}]^{6-}$ at the small pore film at pH 0.3 (see curve "b" on Fig. 4A) and the larger pore film at pH 1 (see curve "c" on Fig. 4B), both situations corresponding to the same "effective pore diameter" of 1.2 nm (Fig. 5A). Of course, the EDL layer is not a truly physical barrier, but rather an anionic zone acting as an electrostatic screening/shielding barrier for preventing effective mass transport of the heteropolyanions through the mesoporous films, from the solution to the underlying electrode surface, but not blocking it totally. For instance, the electrochemical response was not totally suppressed for both POMs at the small pore film electrode at pH 1 (see curves "b" on Fig. 4B&D), even if this situation corresponds to an "effective pore diameter" of 0.4 nm (Fig. 5A). In this case, I_{film}/I_{bare} values of ca. 0.2 (for $[P_2W_{18}O_{62}]^{6-}$) and 0.8 (for $[SiW_{12}O_{40}]^{4-}$) were calculated, suggesting that not only the size but also the charge of the POM can affect the electrochemical response (the more the anion is charged, the stronger the electrostatic barrier is). All the above results and discussion demonstrate the key role of the mesopore diameter in tuning the access of such bulky anionic redox probes to the electrode surface and point out a major influence of ionic strength, which will be further discussed hereafter from H_2SO_4 solutions with added electrolyte (Na_2SO_4).

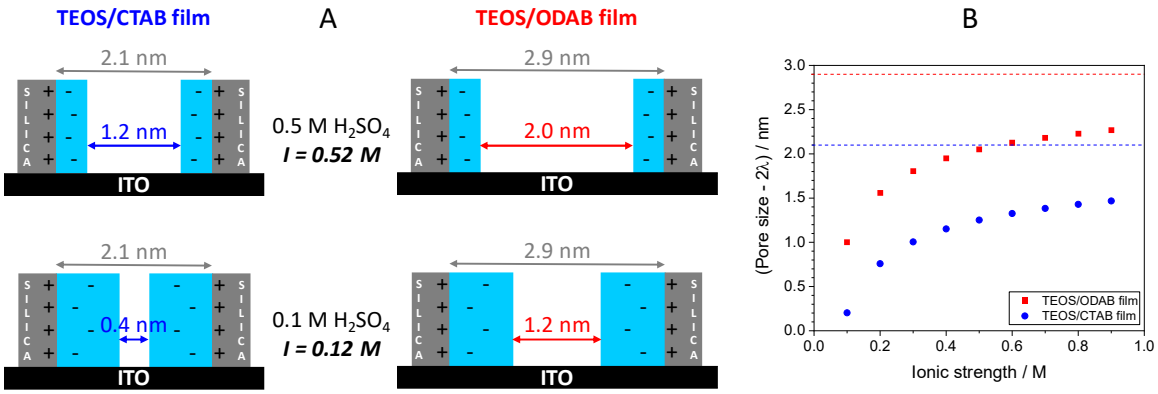

Figure 5. (A) Schematic view of mesopore channels of CTAB- and ODAB-based films with electrical double layers corresponding to pH 0.3 and 1.0. (B) Variation of the effective pore diameters (i.e., "pore size – 2λ" values) of both films as a function of the ionic strength (dashed lines represent the pore diameter of both mesoporous films).

3.4. Effect of the ionic strength

The ionic strength can also be varied by adding a strong electrolyte in the medium. Figure 6 shows typical results obtained with the large pore film electrode (i.e., ODAB-based mesoporous silica) at pH 0.3 and 1.0. Significant variations in peak current intensities (for all $[P_2W_{18}O_{62}]^{6-}$ redox processes) can be seen when adding increasing concentrations of Na_2SO_4 in the medium. In 0.10 M H_2SO_4 (pH 1.0, see Fig. 6C&D&F), I_{film}/I_{bare} values were found to increase from 0.6 in the absence of added electrolyte to 1.1 in the presence of 0.10 M Na_2SO_4, which can be explained by a decrease in the EDL thickness due to a larger ionic strength (changing from 0.12 to 0.42) and making the "effective pore diameter" larger enough (i.e., 2.0 nm in this case) to enable easier ingress of $[P_2W_{18}O_{62}]^{6-}$ species through the nanochannels (and accumulate somewhat in the film). At larger ionic strength, however, this beneficial effect in terms of increasing the "effective pore diameter" is counterbalanced by a competition originating from the presence of larger amounts of SO_4^{2-} anions, limiting thereby the accumulation of $[P_2W_{18}O_{62}]^{6-}$ species and leading to lower I_{film}/I_{bare} values. The optimal ionic strength has thus to be found as the best compromise between a value high enough to keep the EDL as thin as possible (and the free diffusion zone as large as possible in the nanochannels), but not too high to avoid a competition between the electrolyte anions and $[P_2W_{18}O_{62}]^{6-}$ to accumulate in the film. This is consistent with previous observations made for the Keggin POM at a small pore film electrode ($[SiW_{12}O_{40}]^{4-}$ at CTAB-based mesoporous silica film [40]), but the effect is more marked here for the bulkier and more charged $[P_2W_{18}O_{62}]^{6-}$ probe, which needs larger pore film electrode to be evidenced.

When working at pH 0.3, it is impossible to lower the ionic strength below 0.52 M (corresponding to 0.50 M H_2SO_4), and the only observed effect of increasing the Na_2SO_4 concentration of the medium is the competition for accumulation sites (decrease in I_{film}/I_{bare} values, see Fig. 6A&B&E). It is also interesting to compare three cases corresponding to very close values of the "effective pore diameter" of ca. 2.0 nm (i.e., 0.50 M H_2SO_4 corresponding to pH 0.3 (see red curves on Fig. 6A&B), and 0.10 M H_2SO_4 + 0.10 M Na_2SO_4 corresponding to pH 1.0 (see blue curves on Fig. 6C&D) and 0.01 M H_2SO_4 + 0.15 M Na_2SO_4 corresponding to pH 2.0 (data not shown)). In these cases, distinct I_{film}/I_{bare} values were obtained (i.e., 1.8 at pH 0.3, 1.1 at pH 1.0 and 0.8 at pH 2.0), suggesting a more effective $[P_2W_{18}O_{62}]^{6-}$ accumulation via electrostatic attractions at lower pH (due to higher density of $\equiv SiOH_2^+$ groups onto the mesopore walls [54]). On the other hand, the ionic species responsible for adjusting a similar ionic strength in both media are not the same (more monovalent species in the first case, i.e.,

mainly H^+ and HSO_4^-, and much more bivalent SO_4^{2-} in the second and third cases) so that additional competitive binding cannot be excluded in the latter two.

Overall, in addition to the pore dimensions (Fig. 4), many factors are shown to affect the intensity of the voltammetric signals of POMs at mesoporous silica film electrodes in acidic medium (Fig. 6): the pH value itself (defining the binding site density), the ionic strength (controlling the "effective" pore size via variation of the EDL thickness and induced electrostatic shielding) and the concentration of electrolyte anions (likely to compete with $[P_2W_{18}O_{62}]^{6-}$ for binding sites). Even if most data seem to support electrochemical processes based on diffusion-control, one cannot exclude the possibility of charge transfer by electron hopping hopping from POM species adsorbed onto the mesopore walls (as it is the case for redox molecules covalently attached to silica films [44, 61]). This mechanism, if existing here, is certainly not the prominent one because of the weak electrostatic interactions between POM and silica (in agreement with previous observations for electrodes modified with ion exchangers [62, 63]). In addition, the great mobility of POM species is confirmed by their fast desorption when immersing a $[P_2W_{18}O_{62}]^{6-}$-loaded electrode in a POM-free electrolyte solution, leading to a loss of the voltammetric signals (i.e., by ca. 90% in 0.5 M H_2SO_4 + 0.1 M Na_2SO_4), consistent with what was observed for the Keggin-type POM [40].

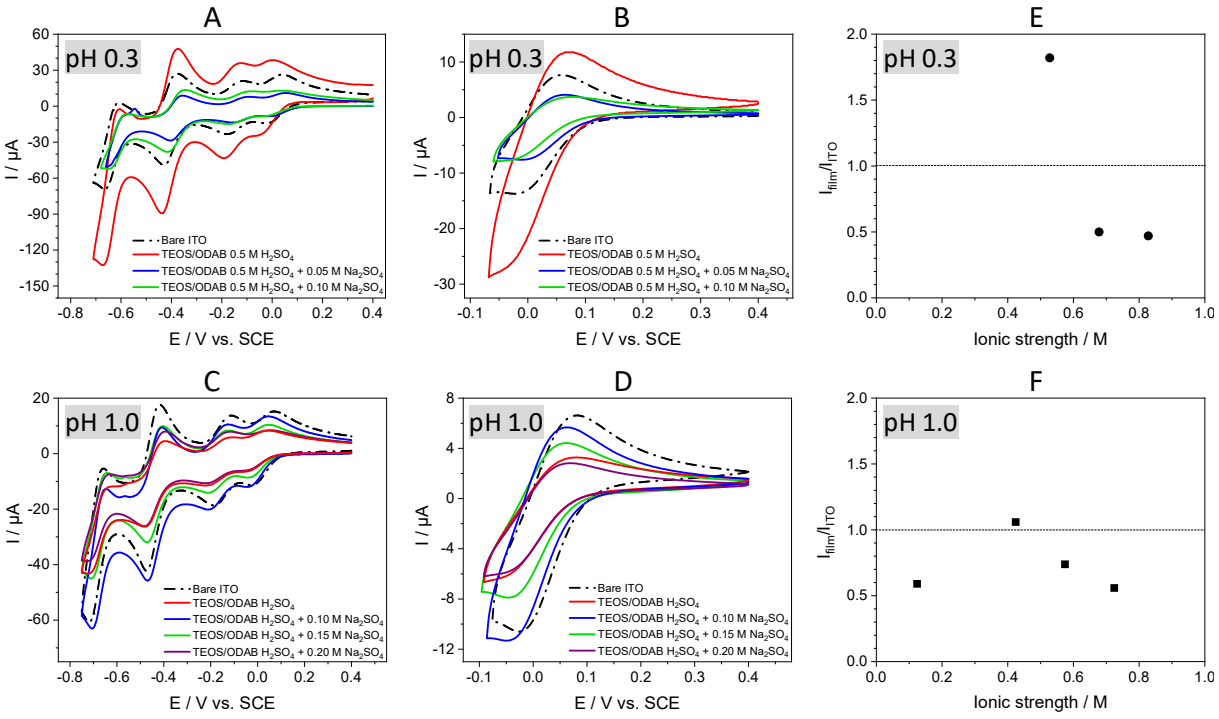

Figure 6. (A-D) Voltammograms recorded in a solution containing 0.5 mM $[P_2W_{18}O_{62}]^{6-}$ and H_2SO_4 at concentrations adjusted to fix the pH to 0.3 (A, B) or 1.0 (C, D) and Na_2SO_4 added at

selected concentrations (0.10, 0.15 or 0.20 M), using a bare ITO electrode and ITO covered with ODAB-based mesoporous silica film (see conditions in insets), at 20 mV s^{-1}. (E, F) Variation of the peak current ratio between film and bare electrodes (I_{film}/I_{bare} values) as a function of the ionic strength, as calculated respectively from data (B, D). Working electrode area: 0.125 cm^2

The above trends were confirmed for the vanadotungstate heteropolyanions also investigated here, $[P_2V_3W_{15}O_{62}]^{9-}$ and $[P_2V_6W_{12}O_{62}]^{12-}$, as illustrated in Figure 7 on the basis of data obtained at pH 1.0 at various ionic strengths. Without added Na_2SO_4 electrolyte, I_{film}/I_{bare} values were lower than for $[P_2W_{18}O_{62}]^{6-}$ (~0.4 for $[P_2V_3W_{15}O_{62}]^{9-}$ and ~0.3 for $[P_2V_6W_{12}O_{62}]^{12-}$, as estimated from the W signals (because those related to the V centers were too ill-defined), compared to 0.6 for $[P_2W_{18}O_{62}]^{6-}$). This fact, associated to peak potentials slightly shifted towards more cathodic values, indicated more impeded mass transport and charge transfer processes for the most highly charged heteropolyanions in the case of small "effective pore diameter" (due to thick EDL on the charged silica walls). But again, adding the Na_2SO_4 electrolyte in the medium led to significant increase in peak currents as a result of more open nanochannels (thinner EDL), providing its concentration was not too high to avoid competition from SO_4^{2-} species for the accumulation sites. This highlighted not only the effect of the charge density of the POM (Note that at the low pH values investigated here, these POMs are expected to be partially protonated (even if the pKa values are unknown for $[P_2W_{18}O_{62}]^{6-}$, $[P_2V_3W_{15}O_{62}]^{9-}$ and $[P_2V_6W_{12}O_{62}]^{12-}$, these species are considered as strong acids [64,65]), but one can reasonably assume a trend of negative charge density following that of the pristine series: $[P_2W_{18}O_{62}]^{6-} < [P_2V_3W_{15}O_{62}]^{9-} < [P_2V_6W_{12}O_{62}]^{12-}$), but also that the main conclusions drawn here should be also valid for other heteropolyanions, which might be of wider interest considering the diversity of electron-rich polyoxometalates and their importance in electrochemistry and beyond [66].

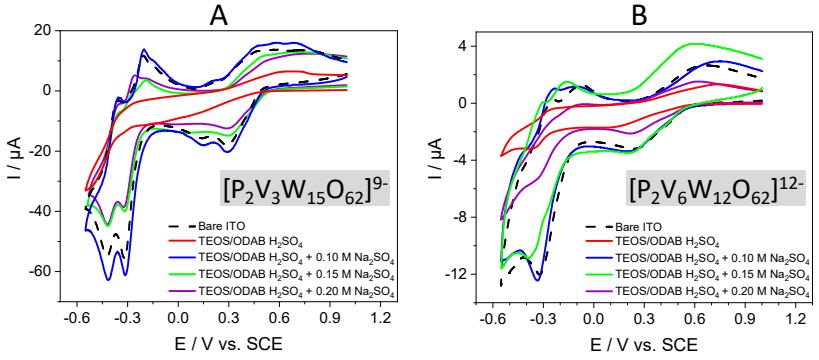

Figure 7. Voltammograms recorded in a solution containing 0.5 mM $[P_2V_3W_{15}O_{62}]^{9-}$ (A) or $[P_2V_6W_{12}O_{62}]^{12-}$ (B) and 0.10 M H_2SO_4 (pH 1.0) to which Na_2SO_4 was added at selected concentrations (0.10, 0.15 or 0.20 M), using a bare ITO electrode and ITO covered with ODAB-based mesoporous silica film (see conditions in insets), at 20 mV s^{-1}. Working electrode area: 0.125 cm^2

4. Conclusions

The presence of mesoporous silica membranes onto an ITO electrode, exhibiting a dense hexagonal packing of vertically oriented nanochanels with monodisperse size, greatly influenced the voltammetric response of the Dawson-type $[P_2V_mW_{18-m}O_{62}]^{n-}$ (m = 0, 3, 6) polyoxometalates (and of a Keggin-type POM, $[SiW_{12}O_{40}]^{4-}$, for comparison purposes). This has been investigated here in acidic media (pH 0.3 - 1.0, where the silica surface is positively charged and thus likely to accumulate POM anions), at various ionic strengths (0.1 - 0.8 M range), and using film electrodes with distinct mesopore diameters (2.1 nm and 2.9 nm). The main factors affecting the intensity of the voltammetric signals are: (1) the membrane pore size, (2) the POM probe charge and size, and (3) the solution pH and ionic strength. The effectiveness of mass transport issues through the mesoporous films, and thus the resulting intensities of the voltammetric signals, is governed by the "effective pore size" of the film resulting from the interplay between the membrane pore diameter and the thickness of the EDL formed onto the silica walls of mesopore channels. This was especially restrictive for bigger and more charged heteropolyanions and when working with small pore film electrodes at low ionic strength, so that only significant electrochemical signals for the quite big and highly charged Dawson-type POMs were obtained with the larger pore film (2.9 nm) and a medium composition with an ionic strength large enough (i.e. ≥0.4 M) to ensure an EDL as thin as possible. Lower pH values also contributed to more effective accumulation, which was however limited at high electrolyte concentration (due to competitive binding). Overall, this work has demonstrated a pH-dependent accumulation behavior, along with a significant pore size- and ionic strength-dependent permselectivity, which was more or less marked depending on the probe size and charge.

Acknowledgements

N.V. is grateful to the CNRS for mobility funding ("CNRS delegation"). The authors thank the CC3M competence center of the University of Lorraine for TEM facilities, as well as the University Paris-Sud / University Paris-Saclay and the CNRS for additional financial help. The work was also supported partly by the french PIA project "Lorraine Université d'Excellence", reference ANR-15-IDEX-04-LUE.

References

[1] M. T. Pope, A. Müller, Polyoxometalate chemistry: an old field with new dimensions in several disciplines, Angew. Chem. Int. Ed. 30 (1991) 34-48. doi:10.1002/anie.199100341.

[2] M. Sadakane, E. Steckhan, Electrochemical properties of polyoxometalates as electrocatalysts, Chem. Rev. 98 (1998) 219-237. doi:10.1021/cr960403a.

[3] D. L. Long, R. Tsunashima, L. Cronin, Polyoxometalates: building blocks for functional nanoscale systems, Angew. Chem. Int. Ed. 49 (2010) 1736-1758. doi:10.1002/anie.200902483.

[4] T. Ueda, Electrochemistry of polyoxometalates: from fundamental aspects to applications, ChemElectroChem 5 (2018) 823-838. doi:10.1002/celc.201701170.

[5] C. Freire, D. M. Fernandes, M. Nunes, M. Araújo, Polyoxometalate-based modified electrodes for electrocatalysis: from molecule sensing to renewable energy-related applications, in: Advanced Electrode Materials, Eds. A. Tiwari, F. Kuralay, L. Uzun, Scrivener Publishing LLC, Beverly, Massachusetts, 2016, Chap. 5, pp. 147-212. doi:10.1002/9781119242659.ch5.

[6] M. Ammam, Polyoxometalates: formation, structures, principal properties, main deposition methods and application in sensing, J. Mater. Chem. A 1 (2013) 6291-6312. doi:10.1039/c3ta01663c.

[7] L. Zhang, Z. Chen, Polyoxometalates: tailoring metal oxides in molecular dimension toward energy applications, Int. J. Energ. Res. 44 (2020), 3316-3346. doi:10.1002/er.5124.

[8] S. M. Wang, J. Hwang, E. Kim, Polyoxometalates as promising materials for electrochromic devices, J. Mater. Chem. C 7 (2019) 7828-7850. doi:10.1039/c9tc01722d.

[9] T. McCormac, D. Farrell, D. Drennan, G. Bidan, Immobilization of a series of Dawson type heteropolyanions, Electroanalysis 13 (2001) 836-842. doi:10.1002/1521-4109(200106)13:10<836::AID-ELAN836>3.0.CO;2-F.

[10] B. Wang, L. Cheng, S. Dong, Construction of a heteropolyanion-modified electrode by a two-step sol-gel method and its electrocatalytic applications, J. Electroanal. Chem. 516 (2001) 17-22. doi:10.1016/S0022-0728(01)00677-5.

[11] P. J. Kulesza, K. Karnicka, K. Miecznikowski, M. Chojak, A. Kolary, P. J. Barczuk, G. Tsirlina, W. Czerwinski, Network electrocatalytic films of conducting polymer-linked polyoxometalate-stabilized platinum nanoparticles, Electrochim. Acta 5 (2005) 5155-5162. doi:10.1016/j.electacta.2005.03.061.

[12] M. Genovese, Y. W. Foong, K. Lian, Designing polyoxometalate based layer-by-layer thin films on carbon nanomaterials for pseudocapacitive electrodes, J. Electrochem. Soc. 162 (2015) A5041-A5046. doi:10.1149/2.0071505jes.

[13] L. Vilà-Nadal, S. G. Mitchell, S. Markov, C. Busche, V. Georgiev, A. Asenov, L. Cronin, Towards polyoxometalate-cluster-based nano-electronics, Chem. Eur. J. 19 (2013) 16502-16511. doi:10.1002/chem.201301631.

[14] Y. Wan, D. Zhao, On the controllable soft-templating approach to mesoporous silicates, Chem. Rev. 107 (2007, 2821-2860. doi:10.1021/cr068020s.

[15] R. Zhang, C. Yang, A novel polyoxometalate-functionalized mesoporous hybrid silica: synthesis and characterization, J. Mater. Chem. 18 (2008) 2691-2703. doi:10.1039/b800025e.

[16] N. R. Shiju, A. H. Alberts, S. Khalid, D. R. Brown, G. Rothenberg, Mesoporous silica with site-isolated amine and phosphotungstic acid groups: a solid catalyst with tunable antagonistic functions for one-pot tandem reactions. Angew. Chem. Int. Ed. 50 (2011) 9615-9619. doi:10.1002/anie.201101449.

[17] F. Bentaleb, O. Makrygenni, D. Brouri, C. Coelho Diogo, A. Mehdi, A. Proust, F. Launey, R. Villanneau, Efficiency of polyoxometalate-based mesoporous hybrids as covalently anchored catalysts, Inorg. Chem. 54 (2015) 7607-7616. doi:10.1021/acs.inorgchem.5b01216.

[18] Y. Leng, Y. Jiang, H. Peng, Z. Zhang, M. Liu, K. Jie, P. Zhang, S. Dai, Heterogeneity of polyoxometalates by confining within ordered mesopores: toward efficient oxidation of benzene to phenol, Catal. Sci. Technol. 9 (2019) 2173-2179. doi:10.1039/c9cy00288j.

[19] D. Feng, J. Wei, M. Wang, Q. Yue, Y. Deng, A. M. Asiri, D. Zhao, Advances in mesoporous thin films via self-assembly process, Adv. Porous Mater. 1 (2013) 164- doi:10.1166/apm.2013.1013.

[20] A. Walcarius, Mesoporous materials and electrochemistry, Chem. Soc. Rev. 42 (2013)

4098-4140. doi:10.1039/C2CS35322A.

[21] D. Fattakhova-Rohlfing, J. Rathousky, Y. Rohlfing, O. Bartels, M. Wark, Funtionalized mesoporous silica films as a matrix for anchoring electrochemically active guests, Langmuir 21 (2005) 11320-11329. doi:10.1021/la051616a.

[22] D. Fattakhova-Rohlfing, M. Wark, J. Rathousky, Electrode layers for electrochemical applications based on functionalized mesoporous silica films, Sens. Actuators B 126 (2007) 78-81. doi:10.1016/j.snb.2006.10.043.

[23] X. Zhang, W. Wu, J. Wang, C. Liu, S. Qian, Molybdenum polyoxometalate impregnated amino-functionalized mesoporous silica films as multifunctional materials for photochromic and electrochemical applications, J. Mater. Res. 23 (2008) 18-26. doi:10.1557/JMR.2008.0028.

[24] T. C. Wei, H. W. Hillhouse, Mass transport and electrode accessibility through periodic self-assembled nanoporous silica thin films, Langmuir 23 (2007) 5689-5699. doi:10.1021/la062699d.

[25] M. Etienne, A. Quach, D. Grosso, L. Nicole, C. Sanchez, A. Walcarius, Molecular transport into mesostructured silica thin films: electrochemical monitoring and comparison between p6m, P63/mmc, Pm3n structures, Chem. Mater. 19 (2007) 844-856. doi:10.1021/cm0625068.

[26] M. Etienne, Y. Guillemin, D. Grosso, A. Walcarius, Electrochemical approaches for the fabrication and/or the characterization of pure and hybrid templated mesoporous oxide thin films: a review, Anal. Bioanal. Chem. 405 (2013) 1497-1512. doi:10.1007/s00216-012-6334-7.

[27] Y. Guillemin, M. Etienne, E. Aubert, A. Walcarius, Electrogeneration of highly methylated mesoporous silica thin films with vertically-aligned mesochannels and electrochemical monitoring of mass transport issues, J. Mater. Chem. 20 (2010) 6799-6807. doi:10.1039/c0jm00305k.

[28] T. Nasir, G. Herzog, N. A. Vodolazkaya, A. Walcarius, Critical effect of film thickness on preconcentration electroanalysis with oriented mesoporous silica modified electrodes, Electroanalysis 31 (2019) 202-207. doi:10.1002/elan201800533.

[29] N. Vilà, E. André, R. Ciganda, J. Ruiz, D. Astruc, A. Walcarius, Molecular sieving with vertically-aligned mesoporous silica films and electronic wiring through isolating

nanochannels, Chem. Mater. 28 (2016) 2511-2514. doi:10.1021/acs.chemmater.6b00716.

[30] D. Fattakhova-Rohlfing, M. Wark, J. Rathousky, Ion-permselective pH-switchable mesoporous silica thin layers, Chem. Mater. 19 (2007) 1640-1647. doi:10.1021/cm062389g.

[31] W. Li, L. Ding, Q. Wang, B. Su, Differential pulse voltammetry detection of dopamine and ascorbic acid by permselective silica mesochannels vertically attached to the electrode surface, Analyst 139 (2014), 3926-3931. doi:10.1039/C4AN00605D.

[32] C. Karman, N. Vilà, A. Walcarius, Amplified charge transfer for anionic redox probes through oriented mesoporous silica thin films, ChemElectroChem 3 (2016) 2130-2137. doi:10.1002/celc.201600303.

[33] T. Nasir, G. Herzog, L. Liu, M. Hébrant, C. Despas, A. Walcarius, Mesoporous silica thin films for improved electrochemical detection of paraquat, ACS Sensors 3 (2018) 484-493. doi:10.1021/acssensors.7b00920.

[34] P. Zhou, L. Yao, K. Chen, B. Su, Silica nanochannel membranes for electrochemical analysis and molecular sieving: a comprehensive review, Crit. Rev. Anal. Chem. (2020), in press (published on line 27 July 2019). doi:10.1080/10408347.2019.1642735.

[35] A. Walcarius, E. Sibottier, M. Etienne, J. Ghanbaja, Electrochemically-assisted self-assembly of mesoporous silica thin films, Nat. Mater. 6 (2007) 602-608. doi:10.1038/nmat1951.

[36] A. Goux, M. Etienne, E. Aubert, C. Lecomte, J. Ghanbaja, A. Walcarius, Oriented mesoporous silica films obtained by electro-assisted self-assemby (EASA), Chem. Mater. 21 (2009) 731-741. doi:10.1021/cm8029664.

[37] Miyata, H.; Kuroda, K. Formation of a continuous mesoporous silica film with fully aligned mesochannels on a glass substrate, Chem. Mater. 12 (2000) 49-54. doi:10.1021/cm990506k.

[38] B. Su, X. Lu, Q. Lu, A facile method to prepare macroscopically oriented mesostructured silica film: controlling the orientation of mesochannels in multilayer films by air flow, J. Am. Chem. Soc. 130 (2008) 14356-14357. doi:10.1021/ja8003254.

[39] Z. Teng, G. Zheng, Y. Dou, W. Li, C. Y. Mou, X. Zhang, A. M. Asiri, D. Zhao, Highly ordered mesoporous silica films with perpendicular mesochannels by a simple Stöber-

solution growth approach, Angew. Chem. Int. Ed. 51 (2012) 2173-2177. doi:10.1002/anie201108748.

[40] N. Vilà, P. de Oliveira, A. Walcarius, I. M. Mbomekallé, pH-modulated ion transport and amplified redox response of Keggin-type polyoxometalates through vertically-oriented mesoporous silica nanochannels, Electrochim. Acta 309 (2019) 209-218. doi:10.1016/j.electacta.2019.03.119.

[41] I.M. Mbomekallé, Y.W. Lu, B. Keita, L. Nadjo, Simple, High Yield and Reagent-Saving Synthesis of Pure α-$K_6[P_2W_{18}O_{62}].14H_2O$, Inorg. Chem. Commun. 7 (2004) 86-90.

[42] R. Contant, M. Abbessi, R. Thouvenot, G. Herve, Dawson Type Heteropolyanions. Syntheses and 31P, 51V, and 183W NMR Structural Investigation of Octadeca(molybdo-tungsto-vanado)diphosphates Related to the $[H_2P_2W_{12}O_{48}]^{12-}$ Anion. Inorg. Chem. 43 (2004) 3597-3604.

[43] R. G. Finke, B. Rapko, R. J. Saxton, P. J. Domaille. Trisubstituted Heteropolytungstates as Soluble Metal Oxide Analogues, 3 Synthesis, Characterization, 31P, 29Si, 51V and 1- and 2-D 183W NMR, Deprotonation, and H^+ Mobility Studies of Organic Solvent Soluble Forms of $H_xSiW_9V3O_{40}^{x-7}$ and $H_xP_2W_{15}V_3O_{62}^{x-9}$. J. Am. Chem. Soc. 108 (1986) 2947-2960.

[44] N. Vilà, A. Walcarius, Electrochemical response of vertically-aligned, ferrocene-functionalized mesoporous silica films: effect of the supporting electrolytes, Electrochim. Acta 179 (2015) 304-314. doi:10.1016/j.electacta.2015.02.169.

[45] S. H. Wu, C. Y. Mou, H. P. Lin, Synthesis of mesoporous silica nanoparticles, Chem. Soc. Rev. 42 (2013) 3862-3875. doi:10.1039/C3CS35405A.

[46] B. Keita, L. Nadjo, New aspects of the electrochemistry of heteropolyacids: Part IV. Acidity dependent cyclic voltammetric behaviour of phosphotungstic and silicotungstic heteropolyanions in water and *N,N*-dimethylformamide, J. Electroanal. Chem. 227 (1987) 77-98. doi:10.1016/0022-0728(87)80067-0.

[47] P. D. Prenzler, C. Boskovic, A. M. Bond, A. G. Wedd, Coupled electron- and proton-transfer processes in the reduction of α-$[P_2W_{18}O_{62}]^{6-}$ and α-$[H_2W_{12}O_{40}]^{6-}$ as revealed by simulation of cyclic voltammograms, Anal. Chem. 71 (1999) 3650-3656. doi:10.1021/ac9814290.

[48] L. Parent, P. A. Aparicio, P. de Oliveira, A. L. Teillout, J. M. Poblet, X. López, I. M.

Mbomekallé, Effect of electron (de)localization and pairing in the electrochemistry of polyoxometalates: study of Wells–Dawson molybdotungstophosphate derivatives, Inorg. Chem. 53 (2014) 5941-5949. doi:10.1021/ic500087t.

[49] Q. Sun, F. Yan, L. Yao, B. Su, Anti-biofouling isoporous silica-micelle membrane enabling drug detection in human whole blood, Anal. Chem. 88 (2016) 8364-8368. doi:10.1021/acs.analchem.6b02091.

[50] A. J. Bard, L. R. Faulkner, Electrochemical Methods: Fundamentals and Applications, John. Wiley & Sons, Inc., New York, NY, 2001, 2nd Ed. ISBN: 978-0-471-04372-0.

[51] P. J. Peerce, A. J. Bard, Polymer films on electrodes. Part II. Film structure and mechanism of electron transfer with electrodeposited poly(vinylferrocene), J. Electroanal. Chem. 112 (1980) 97-115. doi: 10.1016/S0022-0728(80)80011-8.

[52] J. Leddy, A. J. Bard, Polymer Films on electrodes. Part XII: Chronoamperometric and rotating disc electrode determination of the mechanism of mass transport through poly(vinylferrocene) films, J. Electroanal. Chem. 153 (1983) 223-242. doi: 10.1016/S0022-0728(83)80015-1.

[53] Chitosan-assisted fabrication and electrocatalytic activity of the composite film electrode of heteropolytungstate/carbon nanotubes, Electrochim. Acta 55 (2010) 1523-1527. doi:10.1016/j.electacta.2009.10.003.

[54] Y. D. Chiang, H. Y. Lian, S. Y. Leo, S. G. Wang, Y. Yamauchi, K. C. W. Wu, Controlling particle size and structural properties of mesoporous silica nanoparticles using the Taguchi method, J. Phys. Chem. C 115 (2011) 13158-13165. doi:10.1003/jp201017.

[55] A. Malinenko, A. Jonchère, L. Girard, S. Parrès-Maynadié, O. Diat, P. Bauduin, Are Keggin's POMs charged nanocolloids or multicharged anions? Langmuir 34 (2018) 2026-2038. doi:10.1021/acs.langmuir.7b03640.

[56] G. M. Brown, M.-R. Noe-Spirlet, W. R. Busing, H. A. Levy, Dodecatungstophosphoric acid hexahydrate, $(H_5O_2^+)_3(PW_{12}O_{40}^{3-})$. The true structure of Keggin's `pentahydrate' from single-crystal X-ray and neutron diffraction data, Acta Cryst. B33 (1977) 1038-1046. doi:10.1107/S0567740877005330.

[57] M. S. Kaba, I. K. Song, D. C. Duncan, C. L. Hill, M. A. Barteau, Molecular shapes, orientation, and packing of polyoxometalate arrays imaged by scanning tunneling

microscopy, Inorg. Chem. 37 (1998) 398-406. doi:10.1021/ic9705655.

[58] G. Raj, C. Swalus, E. Arendt, P. Eloy, M. Devillers, E. M. Gaigneaux, Controlling the dispersion of supported polyoxometalate heterogeneous catalysts: impact of hybridization and the role of hydrophilicity–hydrophobicity balance and supramolecularity, Beilstein J. Nanotechnol. 5 (2014) 1749-1759. doi:10.3762/bjnano.5.185.

[59] B. Dawson, The structure of the 9(18)-heteropolyanion in potassium 9(18)-tungstophosphate $K_6[P_2W_{18}O_{62}]\cdot 14H_2O$. Acta Cryst. 6 (1953) 113-126. doi:10.1107/S0365110X53000466.

[60] I. K. Song, M. S. Kaba, M. A. Barteau, Nanoscale investigation of mixed arrays of Keggin-type and Wells−Dawson-type heteropolyacids (HPAs) by Scanning Tunneling Microscopy (STM), Langmuir 18 (2002) 2358-2362. doi:10.1021/la0111811.

[61] N. Vilà, J. Ghanbaja, E. Aubert, A. Walcarius, Electrochemically assisted generation of highly ordered azide-functionalized mesoporous silica for oriented hybrid films, Angew. Chem. Int. Ed. 53 (2014) 2945–2950. doi:10.1002/anie.201309447.

[62] T. Wielgos, A. Fitch, A clay-modified electrode for ion-exchange voltammetry, Electroanalysis 2 (1990 449-454. doi:10.1002/elan.1140020606.

[63] A. Walcarius, T. Barbaise, J. Bessière, Factors affecting the analytical applications of zeolite modified electrodes: preconcentration of electroactive species, Anal. Chim. Acta 340 (1997) 61-76. doi:10.1016/S0003-2670(96)00539-9.

[64] B. Keita, Y.-W. Lu, L. Nadjo, R. Contant, Influence of charge distribution on the properties of Keggin- and Dawson-type heteropolyanions. Eur. J. Inorg. Chem. (2000) 2463-2471. doi: 10.1002/1099-0682(200012)2000:12<2463::AID-EJIC2463>3.0

[65] T. Hasegawa, H. Murakami, K. Shimizu, Y. Kasahara, S. Yoshida, T. Kurashina, H. Seki, K. Nomiya. Formation of inorganic protonic-acid polymer via inorganic-organic hybridization: synthesis and characterization of polymerizable olefinic organosilyl derivatives of mono-lacunary Dawson polyoxometalate. Inorg. Chim. Acta (2008) 361, 1385-1394. doi: 10.1016/j.ica.2007.09.002

[66] N. I. Gumerova, A. Rompel, Synthesis, structures and applications of electron-rich polyoxometalates, Nat. Chem. 2 (2018) 0112. doi:10.1038/s41570-018-0112.